Theory and measurements of snores

NOAM GAVRIELY AND OLIVER JENSEN
Department of Mathematics and Statistics, University of Newcastle Upon Tyne, Newcastle NE1 7RU, United Kingdom; Department of Physiology and Biophysics, Faculty of Medicine, and Rappaport Institute for Research in the Medical Sciences, Technion-Israel Institute of Technology, Haifa 31096, Israel; and Biomedical Engineering Department, Northwestern University, Evanston, Illinois 60208

GAVRIELY, NOAM, AND OLIVER JENSEN. *Theory and measurements of snores.* J. Appl. Physiol. 74(6): 2828–2837, 1993.—Upper airway narrowing, collapsibility, and resistance are recognized predisposing factors for snoring and obstructive sleep apnea, but the mechanisms of their action and interaction are not known. We studied a simple theoretical model of the upper airways, consisting of a movable wall in a channel segment that connects to the airway opening via a conduit with a resistance. Inspiratory flow ($\dot{V}$) through the channel segment causes local pressure changes due to viscous losses and the Bernoulli force that may overcome the elastic forces acting on the movable wall. The model predicts instability leading to upper airway closure over a wide range of parameter values. Increasing inspiratory $\dot{V}$ above a boundary, determined by values of upper airway resistance, segment compliance, length, width, and diameter, as well as gas density, leads to a dynamic airway closure. The mathematical model establishes the power relationships between parameters and provides physiologically realistic quantitative simulation of upper airway closure when values are adapted from literature and from radiographic measurements of upper airway motion induced by negative pressure. The rate of appearance of repetitive sound structures during snoring was favorably compared with the model's prediction of the time course of wall motion during collapse. $\dot{V}$ measurements during simulated snores revealed an asymmetric oscillatory pattern compatible with repetitive upper airway closure. We conclude that snoring may be modeled as a series of dynamic closure events of the upper airways. The model predicts that the width and length of the movable portion of the upper airways and the gas density are likely to affect the onset of snoring, in addition to other, previously recognized, parameters.

obstructive sleep apnea; upper airways; breath sounds

SNORES ARE COMMON BREATH SOUNDS produced in adults during sleep (13). They are less commonly encountered in children, except when upper airway narrowing is present (19). The clinical significance of snores is not completely clear. The association between snores and obstructive sleep apnea (OSA) drew attention to their pathophysiology, and several studies were conducted to determine the characteristics of patients with simple ("benign") snores and those who had OSA. These studies led to the documentation of several characteristic features of snoring subjects compared with a normal (control) population of nonsnorers. The relevant parameters identified so far are $\dot{V}$; upper airway diameter, cross section, and shape; upper airway collapsibility and tone; and the flow resistance in the nose and pharynx.

Polygraphic studies of snoring patients have shown that snoring is an inspiratory noise that, very rarely, can persist, even though attenuated, during expiration (13). In studies of the pressure, $\dot{V}$, and noise production during simulated snoring, Perez-Padilla and Remmers (14) noticed that, in general, airflows during snoring exceeded those during noiseless breaths. Thus, sufficient inspiratory $\dot{V}$ has been shown to precipitate the onset of snoring. An unresolved issue is the question of pressure-$\dot{V}$ relationships in the upper airways and, in particular, the possibility of $\dot{V}$ limitation (8, 12).

Roentgenographic measurements of the upper airways made by Hoffstein et al. (6) showed that anterioposterior (AP) airway diameters at the tip of the palate and 1 cm distal to it were significant predictors of snoring but did not distinguish the snorers who did or did not have OSA. Similar studies using the acoustic reflection technique (7) and computed tomography (15) also demonstrated upper airway narrowing. The latter study by Polo et al. showed that non-OSA snorers had significant narrowing at the tongue base and the hyoid bone levels. Thus upper airway narrowing is clearly a factor in the generation of snores. Another interesting observation was recently made by Rodenstein et al. (18), using magnetic resonance imaging, who found that in normal subjects, the pharyngeal cross section had an elliptic shape with its long axis oriented in the coronal plane, whereas in snoring patients the pharynx was either circular or elliptic but with the long axis in the sagittal plane.

The collapsibility of the upper airway has been shown to be increased in patients with OSA during wakefulness (21) and sleep (22). In a recent study, Gleadhill et al. (4) showed that the critical pressure needed for upper airway collapse was significantly less negative in subjects with OSA than in simple snorers. Hoffstein et al. (7) measured pharyngeal distensibility by either applying external positive pressure or changing lung volume and found significant changes with both maneuvers. Thus, upper airway compliance also seems to play a role in snore generation. Oropharyngeal anesthesia, which tends to reduce upper airway tone either by reducing reflex activity or by direct neuromuscular relaxation, has been shown to increase the number of obstructive events in snoring patients (3). The success of nasal continuous positive pressure in relieving OSA (20) and the fact that snoring and OSA almost always occur during sleep when the upper airway muscle tone is reduced indicate the relative importance of upper airway compliance.

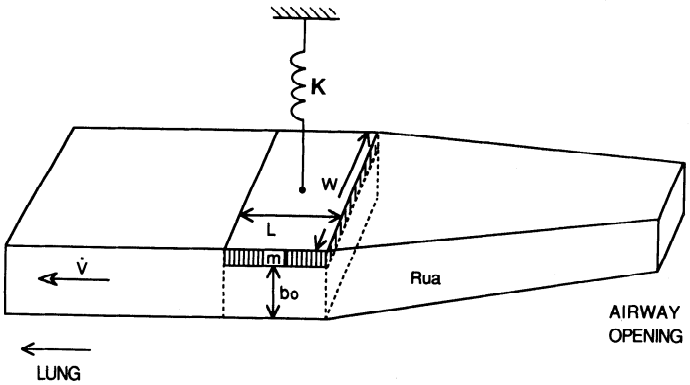

FIG. 1. Schematic diagram of airway model. Rectangular collapsible segment of width W, height b^*, and length L, with 1 wall supported by spring with elastic constant K, is connected to rigid upper airway having resistance (Rua) to flow ($\dot{V}$).

The importance of upper airway resistance (Rua) as a factor in the generation of snores and in some cases of OSA has been recognized for a long time (11, 17). This led to attempts to reduce Rua by nasal septum surgical procedures as a method to alleviate OSA (13). These operations were successful only for some of the patients, with no apparent ability to predict who would benefit more than others.

These clinical and physiological data point out several parameters as contributing to the generation of snores. These are the respiratory $\dot{V}$, upper airway (pharyngeal) cross-sectional area and/or diameter, upper airway (pharyngeal) collapsibility, and Rua. The relative importance of each parameter and the interactions between them have not yet been resolved. In this study, we present a simplified model of the upper airways, which takes into account the parameters listed above, as well as the dimensions of the collapsible airway section and the density of the gas. A mathematical analysis of the model is used to generate predictions of the relative contribution of each of the parameters. Measurements of airway wall motion and of snoring sounds and $\dot{V}$ during simulated snores were used to provide values for the model's parameters and to test specific predictions of the model.

MODEL AND MODEL RESULT

Figure 1 shows a schematic representation of the upper airways. A collapsible segment is represented as a section of length L with a cross section approximated as a rectangle of width W (i.e., lateral diameter) and depth b^* (i.e., AP diameter). The moveable wall of the collapsible segment is assumed to have a mass m and to be supported by a linear spring with a Hooke spring constant K; the spring's neutral position is when $b^* = b_0$. It is further assumed that the moving wall of the collapsible section maintains its parallel orientation with respect to the opposing wall at all times. A constant mean $\dot{V}$ is assumed in the inspiratory direction. The upper airways, from the collapsible section to the airway opening, are assumed to have a linear flow resistance (Rua).

The intra-airway pressure in the collapsible segment has two components, a pressure drop due to the viscous resistance of the upper airways ($P_R = \dot{V}Rua$) and a Bernoulli-effect pressure across the collapsible segment ($P_B = {}^1/_2\rho U^2$, where ρ is the gas density and $U = \dot{V}/Wb^*$ is the gas velocity). The subatmospheric pressure beneath the movable wall tends to pull it closer to the opposing wall and to reduce b^*. The pressure has to be multiplied by the area LW of the plate on which it is acting to be expressed as the sum of two forces, $F_R = P_R LW = \dot{V}RuaLW$ and $F_B = P_B LW = {}^1/_2\rho U^2 LW$. The opposing force that balances the closure is the elastic force $F_E = K(b_0 - b^*)$. As long as the opposing forces are equal, the sum of the forces is zero. However, if any of the forces overcomes the others, the plate will be set into motion. Thus, the equation of motion of the plate is given by

$$m\frac{d^2b^*}{d(t^*)^2} = F_E - F_R - F_B \qquad (1)$$

where t^* is the (dimensional) time. Explicitly, *Eq. 1* becomes

$$m\frac{d^2b^*}{d(t^*)^2} = Kb_0\left(1 - \frac{b^*}{b_0}\right) - \dot{V}RuaLW - \frac{1}{2}\rho\left(\frac{\dot{V}}{Wb^*}\right)^2 LW \qquad (2)$$

where $d^2b^*/d(t^*)^2$ is the acceleration of the moveable plate toward the opposing wall. The maximal elastic force is expected to be $F_{E0} = Kb_0$ when the segment is completely collapsed (i.e., $b^* = 0$).

The model contains eight parameters, but because they arise only in certain algebraic combinations in *Eq. 2*, they do not all have independent effects. If we define the following nondimensional quantities, however

$$b = \frac{b^*}{b_0}; \quad t = t^*\left(\frac{K}{m}\right)^{1/2};$$
$$\mu = \frac{F_{B0}F_{E0}}{F_R^2} = \frac{\rho K}{Rua^2W^3b_0L}; \qquad (3)$$
$$q = \frac{F_R}{F_{E0}} = \frac{\dot{V}RuaWL}{b_0K}$$

where $F_{B0} = {}^1/_2\rho LW(\dot{V}/Wb_0)^2$, then *Eq. 2* becomes

$$\frac{d^2b}{dt^2} = 1 - b - q - \frac{\mu q^2}{2b^2} \qquad (4)$$

Equation 4 shows that the model is governed by only two independent parameters, μ and q: q represents the head-loss force normalized by F_{E0}, whereas μq^2 is the inertial force F_{B0} when the tube is fully open normalized by F_{E0}. For simplicity we use *Eq. 4* in our analysis, but we return to dimensional quantities when discussing the results.

Solution structure. The function on the right-hand side of *Eq. 4*, $f(b;q,\mu) = 1 - b - q - \mu q^2/2b^2$, determines the behavior of the moveable wall. If f is positive the plate will accelerate outward (or decelerate inward), if f is zero an equilibrium is possible, and if $f < 0$ the segment will either collapse or decelerate outward, depending on b. Figure 2 shows a family of curves of f vs. b. For $q = 0$ (i.e., the viscous and inertial forces are zero because $\dot{V}$ is zero), $f = 1 - b$ and the plate will be stable at $b = 1$ ($b^* = b_0$). For

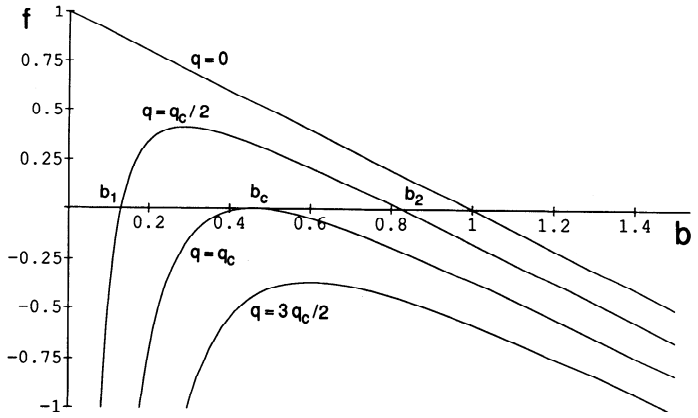

FIG. 2. Dimensionless wall acceleration ($f = 1 - b - q - \mu q^2/2b^2$) plotted for $\mu = 1$ as function of dimensionless wall position b for selected values of dimensionless flow q. Critical q (q_c) is defined as value of q for which maximum of f lies on b axis ($f = 0$) at $b = b_c$ (where b_c is critical wall position). b_1 and b_2 are solutions of f for which plate is stationary.

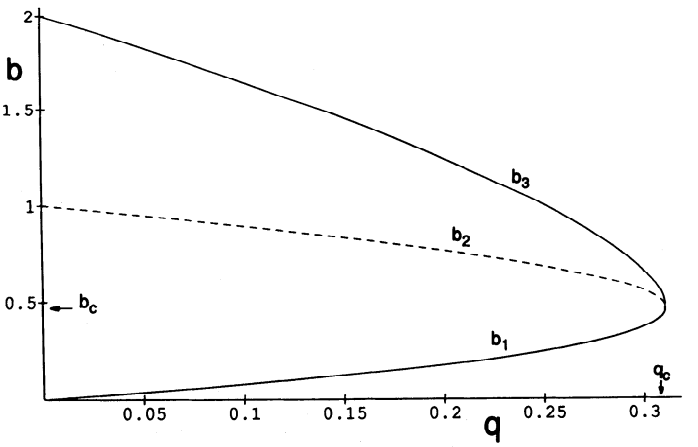

FIG. 4. Dimensionless wall positions b_1 (bottom solid line), b_2 (dashed line), and b_3 (top solid line, defined in *Eq. 6*) plotted as functions of dimensionless q for $\mu = 1$. b_1 and b_2 correspond to steady solutions b_1 and b_2 in Fig. 2. For any given $q < q_c$, if wall is released from rest with initial b lying between b_1 and b_3, then channel will remain open, oscillating around equilibrium position b_2.

$q > 0$, f has a maximum at $b = (\mu q^2)^{1/3}$. This maximum (f_{max}) may be positive ($f_{max} > 0$, e.g., the curve $q = q_c/2$ in Fig. 2, where q_c is the critical q); in this case, $f = 0$ at b_1 and b_2 and $f < 0$ for $b < b_1$ where segment closure is expected or for $b > b_2$ where there is outward deceleration. If $f_{max} < 0$, the channel will ultimately collapse regardless of the value of b (e.g., the curve for $q = 3q_c/2$ in Fig. 2). A limiting case is when $f_{max} = 0$ (the curve $q = q_c$ in Fig. 2). This happens when $q = q_c(\mu)$, where the relationship between q_c and μ is given by

$$\mu = \frac{8}{27}\frac{(1 - q_c)^3}{q_c^2} \qquad (5)$$

The corresponding zero of f lies at the critical b (b_c) = $(\mu q_c^2)^{1/3} = {}^2/_3(1 - q_c)$. Figure 3 shows the relationships between q_c, b_c, and μ. Note that as μ increases from 0, q_c rapidly decreases and b_c rapidly increases. The behavior of the two roots of $f = 0$, $b_1(q,\mu)$ and $b_2(q,\mu)$ (these were computed using Newton's method), is shown in Fig. 4;

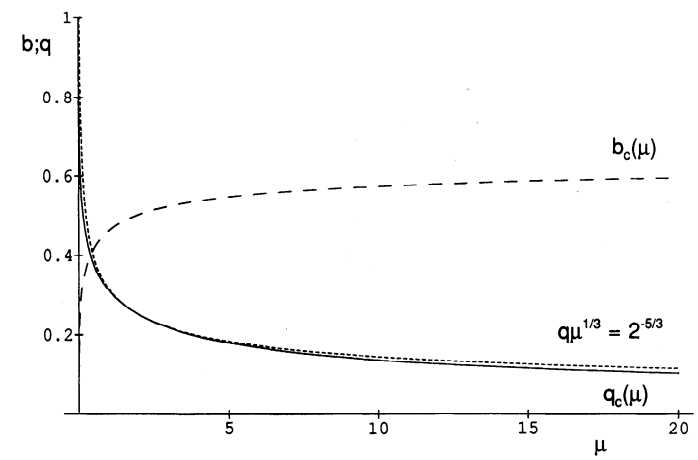

FIG. 3. Curves of dimensionless q_c (solid line) and dimensionless b_c (dashed line) plotted as functions of μ. For any given value of μ, a value of q that is above q_c curve will inevitably lead to collapse and closure. Also shown is curve $q\mu^{1/3} = 2^{-5/3}$ (dotted line, see *Eq. 8*), which provides good approximation to $q = q_c(\mu)$.

the roots coalesce at $b = b_c$ when $q = q_c$ (Figs. 2 and 4). As q goes to 0, b_1 approaches 0 and b_2 approaches 1.

b_1 and b_2 are two steady solutions of *Eq. 4*. To determine whether they represent stable or unstable equilibria and to understand the unsteady solutions of *Eq. 4*, we consider the behavior of trajectories in the (b,db/dt)-phase plane (Fig. 5, *A–C*), where (b_1,0) is a saddle point and (b_2,0) is a center. (An account of phase-plane techniques is given in Ref. 9.) Each trajectory in the phase plane represents a solution of *Eq. 4*, with time increasing in the direction of the arrows. The closed trajectory around (b_2,0) in Fig. 5*A* represents indefinite oscillation of the channel wall around the equilibrium position $b = b_2$. For the solutions of *Eq. 4* represented by trajectories such as the outermost one in Fig. 5*A*, b ultimately decreases to 0 as time increases, representing complete closure of the airway. This is shown explicitly in Fig. 5*B*, where the time evolution of each solution is plotted as b vs. t; these curves were computed numerically with a fourth-order Runge-Kutta scheme, in each case using the initial condition $db/dt = 0$. Figure 5*A* shows that the equilibrium at $b = b_1$ is not stable, since a small deviation from the equilibrium will lead ultimately either to closure [if the deviation takes the system to a point outside the closed trajectory through the saddle point (b_1,0)] or to oscillations around $b = b_2$ (if the system is perturbed to a point within this closed trajectory). The closed trajectory through (b_1,0) therefore separates the two classes of solutions, oscillatory or those representing closure. the trajectory intersects $db/dt = 0$ at $b = b_3$, where $b_3(\mu,q)$ is determined by integrating *Eq. 4* once, and is given by

$$b_3 = 1 - q - \frac{b_1}{2} + \sqrt{\left(1 - q - \frac{b_1}{2}\right)^2 - \frac{\mu q^2}{b_1}} \qquad (6)$$

$b_3(\mu,q)$ is plotted as a function of q in Fig. 4. This trajectory is effectively a boundary of stability. If the channel wall is released from rest with $b < b_1$, the segment will collapse with increasing velocity. It will also collapse if the wall is perturbed beyond b_3 and allowed to spring back.

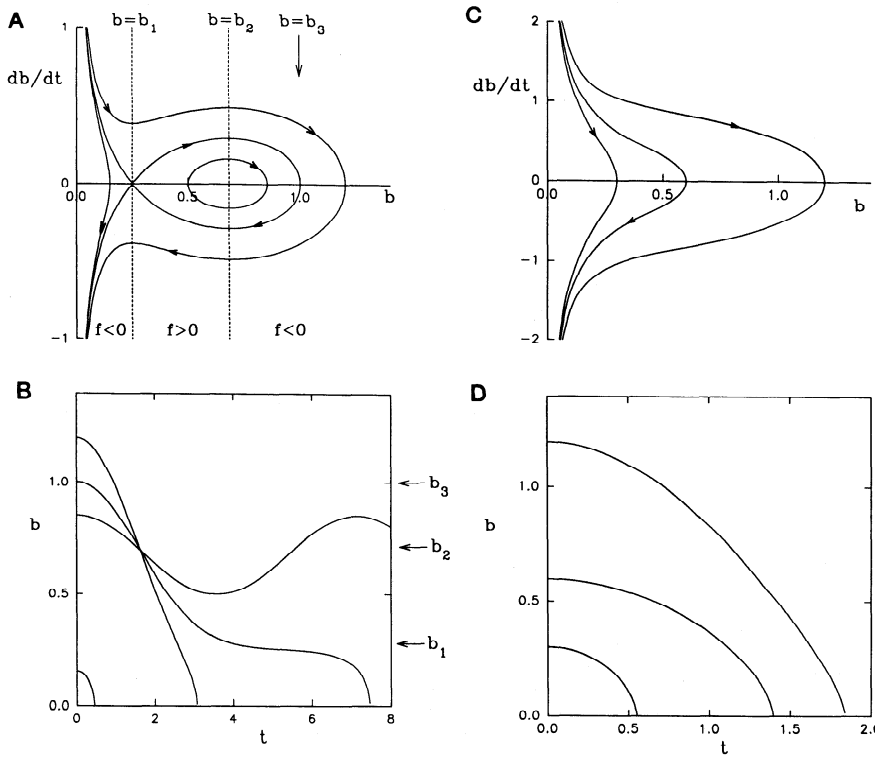

FIG. 5. *A* and *C*: dimensionless wall velocity db/dt vs. dimensionless b in phase-plane presentation. Trajectories represent solutions of *Eq. 4* for $\mu = 1$, $q = 0.25$ (i.e., $q < q_c$; *A*) and $\mu = 1$, $q = 0.5$ (i.e., $q > q_c$; *C*). Arrows show direction of increasing time. Points b_1 and b_2 correspond to those in Figs. 2 and 4; b_3 is shown in Fig. 4. Sign of dimensionless acceleration $f = d^2b/dt^2$ is given next to curves. Time evolution of b as represented by each trajectory in *A* and *C* is shown *B* and *D*, respectively; in every example $db/dt = 0$ at $t = 0$.

Thus a stable equilibrium (b_2) exists provided $0 \leq q \leq q_c(\mu)$ (Fig. 5, *A* and *B*); for $q > q_c$ (Fig. 5, *C* and *D*), no equilibria exist and b decreases to zero in finite time for all initial conditions.

Stability of the channel. Stability of the channel is determined by two parameters, μ and q. If $q < q_c(\mu)$, then a stable equilibrium exists (b_2, dashed line in Fig. 4); closure occurs only if b is perturbed sufficiently far from this equilibrium solution, e.g., if $b < b_1$ or $b > b_3$ (Fig. 5, *A* and *B*). If $q > q_c$, i.e., for points lying above the solid curve in Fig. 3, closure is inevitable. The maximum value of q_c is 1, which occurs for $\mu \rightarrow 0$ (Fig. 3): thus if $q > 1$, i.e., if

$$\frac{\dot{V}\text{Rua}WL}{b_0K} > 1 \qquad (7)$$

then closure will definitely occur. This condition is independent of both the mass of the wall and the mass of the fluid; it says essentially that if Rua is sufficiently large, the airway pressure on inspiration is sufficiently negative to overcome the stabilizing elastic forces. If $q < 1$, then the condition for instability [$q > q_c(\mu)$] depends additionally on the density of the fluid through μ, where μ is given by *Eq. 3*, and expresses how pressure reduction in the airway due to both viscous and Bernoulli effects overcomes elastic forces. Increasing either μ or q destabilizes the airway by increasing the size of both the inertial and the viscous forces. When μ is small, Fig. 3 shows that an increase in μ will be more likely to destabilize the airway than an increase in q; when μ is large, an increase in q will be more dangerous. (The wall segment mass m never appears in stability conditions but arises in estimates of closure time.)

Variations of individual parameters. With the stability of the airway having been determined with respect to the nondimensional groups μ and q (3), the effects of changing the individual parameters $\dot{V}$, b_0, L, W, K, Rua, and ρ are now determined. We do this by examining how q and μ vary with respect to the stability boundary $q = q_c(\mu)$ (Fig. 3) as each dimensional parameter is varied in turn. To test the model with the use of dimensional parameters, we examine variations of the parameters around the following approximate "baseline" values: $\dot{V} = 10^3$ cm^3/s, $b_0 = 0.6$ cm, $L = 6$ cm, $W = 1$ cm, $K = 3.6 \times 10^5$ g/s^2, Rua = 10 g · cm^{-4} · s^{-1}, $\rho = 10^{-3}$ g/cm^3, and $m = 10$ g. The values of b_0, L, and K were determined from X-ray measurements in a normal upright subject (see EXPERIMENTAL METHODS). From *Eq. 3*, these values correspond to $q \approx 0.3$, $\mu \approx 1$, a point that, encouragingly, lies closely over $q = q_c(\mu)$ in Fig. 3. We replot the stability boundary $q = q_c(\mu)$ in graphs of $\dot{V}$ vs. ρ, $\dot{V}$ vs. b_0, $\dot{V}$ vs. K/L, and $\dot{V}$ vs. W (Fig. 6, *A–D*, respectively); in each case we let Rua take the values 2, 5, 10, and 20 g · cm^{-4} · s^{-1} while holding the four remaining variables constant at their baseline values.

Increasing $\dot{V}$ causes q to increase but causes μ, being independent of $\dot{V}$, to remain constant. This leads to a transition from a state in which a stable equilibrium exists [e.g., $q < q_c(\mu)$ in Fig. 3] to a state in which none exists [$q > q_c(\mu)$], thus causing closure. This is evident in Fig. 6, *A–D*: increasing $\dot{V}$ (with all other parameters held fixed) always takes the system above the stability boundary into an unstable regime.

Decreasing ρ (i.e., breathing a He-O_2 mixture instead of air) keeps q constant but decreases μ. Thus for $q < 1$, a transition from an unstable to a stable state may be observed; this is demonstrated explicitly in Fig. 6*A*. Notice that the more ρ is reduced, the greater the increase in $\dot{V}$ required to guarantee closure. This is a testable prediction of the model, as He-O_2 may be substituted for air in

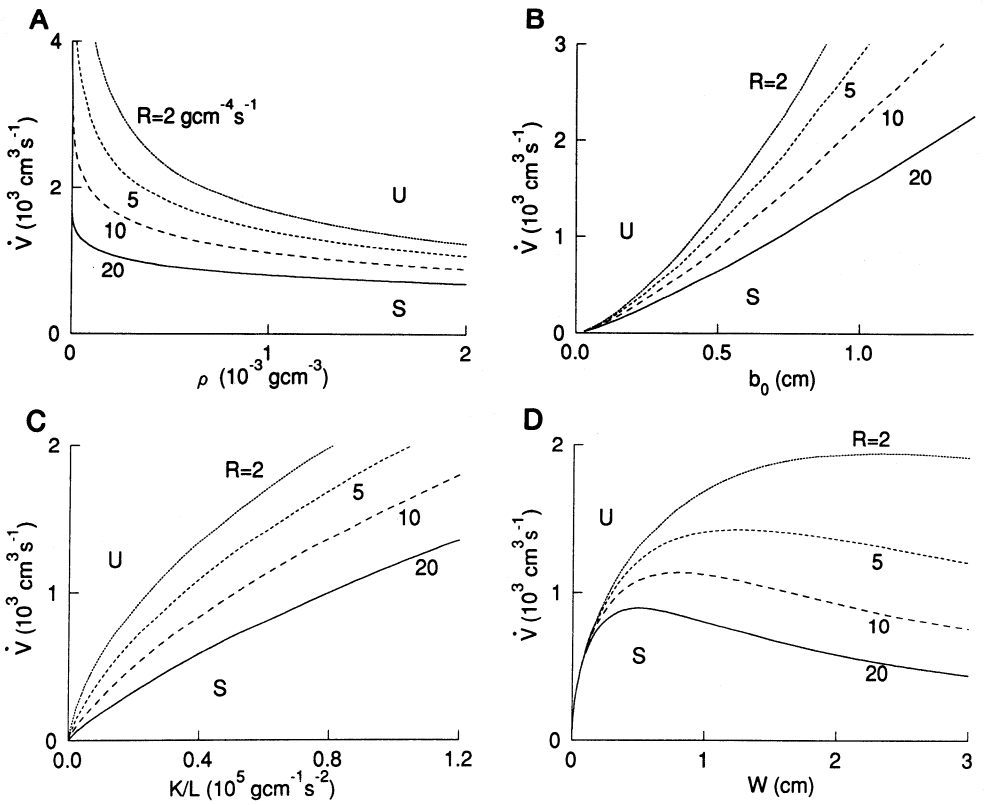

FIG. 6. Stability boundary $q = q_c(\mu)$ is plotted in terms of following pairs of dimensional parameters: $\dot{V}$ and ρ (*A*), $\dot{V}$ and b_0 (*B*), $\dot{V}$ and K/L (*C*), and $\dot{V}$ and W (*D*). These curves are plotted for Rua (R) = 2, 5, 10, and 20 $g \cdot cm^{-4} \cdot s^{-1}$ in each case. In each panel, 4 remaining dimensional parameters that were held fixed all took baseline values given in text. Beneath each curve a stable equilibrium state exists (S); above each curve closure is inevitable (U).

heavy snorers or OSA patients while snoring or apnea score is recorded. Conversely, it is predicted that hyperbaric conditions will be associated with increased incidence of snoring and OSA. In high altitudes, where ρ is smaller, snoring may be less common if $\dot{V}$ does not increase with the need to raise alveolar ventilation.

Reducing the neutral AP diameter b_0 of the collapsible segments increases both q and μ, leading to a transition from a stable to an unstable configuration (Fig. 6*B*). This is a well-recognized predisposing factor for snore generation and OSA as outlined in the introduction.

Increasing Rua reduces the pressure beneath the wall and always ultimately induces closure; this destabilizing effect is demonstrated clearly in Fig. 6, *A–D*, in which increasing Rua increases the extent of the unstable regime. More specifically, increasing Rua causes q to increase but μ to decrease, subject to the condition that $q\mu^{1/2} = (\dot{V}^2 L\rho/b_0^3 KW)^{1/2}$ ($=a_R$, say) remains constant. The stability of the channel is therefore governed by the relationship between the curves $q = q_c(\mu)$ and $q = q_R(\mu) \equiv a_R/\mu^{1/2}$. At large μ, q is sufficiently small that *Eq. 5* can be approximated by $q_c \approx {}^2/_3{}^{3/2}/\mu^{1/2}$, so $q_R(\mu) > q_c(\mu)$ as $\mu \to \infty$ provided $a_R > {}^2/_3{}^{3/2}$ (=0.54). This condition is sufficient to guarantee that $q_R(\mu) > q_c(\mu)$ for all μ, indicating that closure is always inevitable. For $a_R < {}^2/_3{}^{3/2}$, stable states exist at sufficiently large values of μ [where $q_R(\mu) < q_c(\mu)$], but increasing Rua sufficiently will always reduce μ enough for $q_R(\mu)$ to eventually exceed $q_c(\mu)$, resulting in closure.

The effect of increasing L (i.e., increasing the area of the wall over which destabilizing pressure acts) or decreasing K (i.e., making the wall less rigid and therefore more prone to close) is always ultimately to cause the channel to undergo complete collapse, as shown in Fig. 6*C*. This is proved as follows: reducing K/L causes q to increase or μ to decrease, with $q\mu = (\dot{V}\rho/b_0^2 W^2 \mathrm{Rua})$ ($=a_L$, say) remaining constant. By choosing μ sufficiently large, $q_L(\mu) = a_L/\mu$ can always be made smaller than $q_c(\mu)$, but reducing μ will always cause $q_L(\mu)$ to exceed $q_c(\mu)$, thus resulting in closure.

The effect of varying W is demonstrated in Fig. 6*D*, which shows that the stability boundary in the $(\dot{V},W)$ plane has a maximum. Starting from a point beneath the boundary, increasing W causes closure because widening the collapsible segment increases the area over which destabilizing pressures act; decreasing W causes closure because narrowing the channel sufficiently increases the velocity at the constriction and so raises the destabilizing inertial force. (From Fig. 6*D* it appears that destabilization due to W being too large is the more likely scenario for physiological parameter values.) A more precise argument is as follows: increasing W causes q to increase and μ to decrease, keeping $q\mu^{1/3} = (\dot{V}^3 \mathrm{Rua} L^2\rho/K^2 b_0^2)^{1/3}$ ($=a_W$, say) constant, so that stability is determined by the relationship between the curves $q = q_c(\mu)$ and $q = q_W(\mu) \equiv a_W/\mu^{1/3}$. If $a_W > 2^{-5/3}$ (=0.31), then $q_W(\mu) > q_c(\mu)$ for all μ, in which case closure will occur. It is straightforward to show that $q = q_W(\mu)$ and $q = q_c(\mu)$ meet tangentially at $q = {}^1/_4$, $\mu = 2$ if $a_W = 2^{-5/3}$ (see Fig. 3). For $a_W < 2^{-5/3}$, there exists a range of μ for which a stable state exists (corresponding to a region beneath the hump in a each curve in Fig. 6*D*), but either increasing or decreasing μ sufficiently will lead to closure.

There are therefore a number of simple conditions that guarantee instability: $q > 1$ (see *Eq. 2*), $q\mu^{1/2} > {}^2/_3{}^{3/2}$ (see *Eq. 4*), and $q\mu^{1/3} > 2^{-5/3}$ (see *Eq. 5*). These conditions are

all independent of m and independent of ρ, R, and W, respectively. It turns out that for $\mu < 10$, say, the latter condition

$$\left(\frac{32\dot{V}^3 \mathrm{Rua} L^2 \rho}{b_0^2 K^2}\right)^{1/3} > 1 \qquad (8)$$

comes remarkably close to the condition $q > q_c(\mu)$ (see Fig. 3, dotted line), and because it is so simple it is probably the most useful for physiological conditions.

Closure time. There are three time scales in this problem: the nondimensional elastic time scale T_e, which is a quantity of unit order of magnitude in the chosen scalings [Ref. 3; in dimensional units it is $(m/K)^{1/2}$, which by use of the parameter values given previously is 0.005 s]; the nondimensional inertial time scale $T_i = (\mu q^2)^{-1/2}$ [in dimensional units $(b_0^3 mW/L\rho\dot{V}^2)^{1/2} \approx 0.02$ s by use of the parameter values above]; and a time scale for closure encouraged by resistance $T_r = q^{-1/2}$ [in dimensional units $(mb_0/\mathrm{Rua}LW\dot{V})^{1/2}$ or 0.01 s by use of the parameter values above]. These time scales can be used to give rough estimates of the closure time (T_c) in certain regimes. When inertial forces dominate, for example (i.e., $\mu q^2 >> 1$ and $\mu q^2 >> q$ or when b becomes very small), then we can expect $T_c \approx T_i$. If $q >> 1$ but $\mu q^2 << q$, so that the effects of the upstream viscous resistance dominate, then $T_c \approx T_r$. For the parameter values given above, however, both inertial and viscous effects are important in controlling the closure process, and near the threshold of stability ($q = q_c$) elastic forces will provide significant hindrance to closure. (This is made particularly clear in Fig. 5*B*, which shows how, for a given μ and $0 < q < q_c$, the behavior of the nondimensional channel diameter b as a function of nondimensional time t is very strongly dependent on the initial value of b, i.e., on the strength of the initial elastic forces.) Nevertheless, beyond this threshold, T_c can be expected to be on the order of 0.01–0.1 s; subsequent reopening (if due to elastic forces alone) can be expected to be more rapid.

Damping. In the presence of damping, *Eq. 4* becomes

$$\frac{d^2b}{dt^2} + \delta\frac{db}{dt} = 1 - b - q - \frac{\mu q^2}{2b^2} \qquad (9)$$

where δ is a damping parameter, assumed to be small and positive. The values of q_c, b_1, and b_2 are unaltered by δ. There is a weak perturbation to the phase plane when $0 < q < q_c$ (Fig. 5*A*) such that b_2 becomes a stable focus, and the trajectory connecting b_1 and b_3 is altered slightly so that it spirals clockwise into b_2. This means that oscillations about $b = b_2$ will all eventually decay to the equilibrium, as would be expected. Weak damping has no significant effect on trajectories representing closure of the airway and, most significantly, it has no effect whatsoever on the global stability results (Figs. 3 and 6).

EXPERIMENTAL METHODS

Measurements of snoring sounds were made in two men during sleep and during production of simulated snore sounds and in six anesthetized dogs with experimentally induced upper airway constriction caused by inflating an implanted submucosal balloon (1). Sounds were picked up using an audio microphone (Shure) hung 30 cm above the head of the sleeping subject or by a contact sensor (piezoelectric, Rappaport Inst. Tech. Unit, Haifa, Israel) secured to the neck in the awake human and anesthetized dogs studies. The signals were amplified and digitized into the computer (MacIntosh SE computer, Sound Cap analog-to-digital converter, 8 bit, at sampling rates of 5.5 and 11 kHz). The sound signals were analyzed in the time domain by identifying and counting the number of repetitive sound structures per unit time.

In addition to the analysis of snoring sounds, we measured the static upper airway compliance, dynamic $\dot{V}$, and esophageal pressure in a normal subject who simulated a snore. Compliance measurements were made with the subject standing. Lateral X-ray views of the neck were taken with the subject relaxed during breath hold and with the subject producing -24 cmH_2O of static negative pressure measured with a water manometer connected to the right nostril while the other nostril and the mouth were closed. Calibration was done by taping a coin of known size to the skin overlying the cricoid cartilage at the midline.

$\dot{V}$ measurements during simulated snores were made with the subject standing. An esophageal balloon was inserted and connected to a differential pressure transducer (Valydine MP-45, 6–28 membrane). $\dot{V}$ was measured using a pneumotachograph (Fleish no. 0, Gould) coupled to a solid-state differential pressure transducer (Microswitch model 163) with a very-high-frequency response (flat response to 1 kHz). The use of this transducer was essential to provide an adequate recording of the details of the $\dot{V}$ patterns. The data were sampled into the computer (AST computer, 286 processor) via an ana-

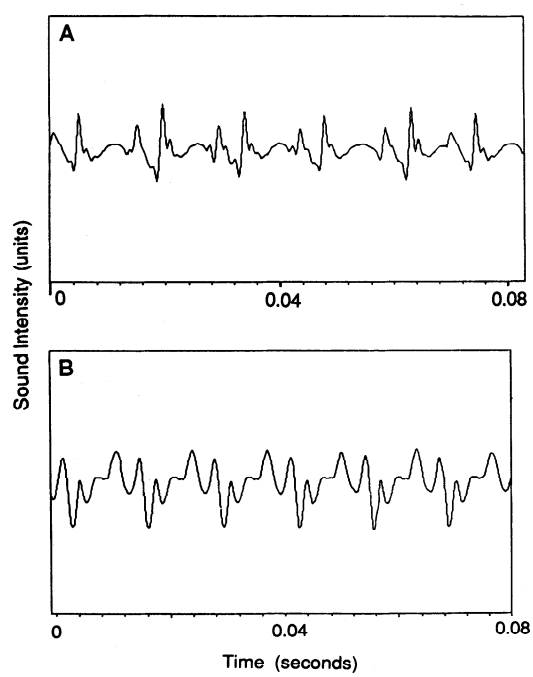

FIG. 7. Typical snoring sounds. Note repetition of basic sound structures at rate of 71 Hz (*A*) and 75 Hz (*B*).

log-to-digital converter (ADA 1100 ±12 bit, Realtime Devices, State College, PA) at 1,000 samples/s.

EXPERIMENTAL RESULTS

Snoring sounds, recorded from sleeping and awake men and from dogs with upper airway obstruction, had a common feature, repetition of a complex sound structure at regular intervals. Figure 7 shows typical examples of snoring sounds. The rate of repetition was found to be 30–100/s. The shapes of the individual structures varied among the subjects and the dogs and also within each subject or dog. A common pattern had one to three spikes (i.e., sharply peaked waves) followed by a wave (i.e., a rounded sound structure). The number of structures per unit time was the same as the $\dot{V}$ oscillations observed in the $\dot{V}$ signal in the awake subject who simulated snores. Figure 8 shows segments of $\dot{V}$ in an expanded time scale. The important feature of the $\dot{V}$ oscillation, clearly shown in Fig. 8, is the asymmetry of the wave form. In each cycle $\dot{V}$ is sharply reduced to a value that is just slightly higher than zero.

Figure 9 shows lateral neck X-ray plates during a relaxed state and during static inspiratory effort of −24 cmH_2O. Line drawings of the upper airway contour are also shown. Upper airway narrowing is prominent in the naso- and oropharynx and at the hyoid bone level. The posterior wall of the pharynx moved forward by 2–4 mm over a 6-cm length. Thus an approximate estimate of the upper airway compliance K is 0.01 cm/cmH_2O. The AP diameter of the airways was smallest at the hyoid bone level and was 0.6 cm in the relaxed state and 0.2 cm when negative pressure was applied.

DISCUSSION

The simple model of upper airway wall stability presented here analyzes the conditions that lead to $\dot{V}$-induced collapse and closure. Once the airway collapses, it may remain closed as in OSA or repetitively reopen and close as in snores. This is dependent on the elastic properties of the airway wall, the pressure generated in the lungs, and the liquid adherence surface forces between the opposing collapsed walls. The model shown here does not address the reopening issue. The model incorporates the mechanical properties of the system to predict their influence on upper airway closure. Although the airway diameter and stiffness, Rua, and $\dot{V}$ are well known to influence the stability of the upper airways, this model predicts that ρ and L will also affect its collapsibility. We were unable to find clinical or experimental data to evaluate these predictions. When normal values were given to the parameters, the model predicts upper airway stability. However, it is easy to see that by substituting slightly higher values for $\dot{V}$, Rua, L, or ρ or smaller values for b_0 or K supercritical conditions and instability are rapidly reached. We carried out the X-ray measurement of the upper airway static compliance to obtain an estimate of normal values of b_0 in the relaxed state, K, and L. The latter value was not available in the literature.

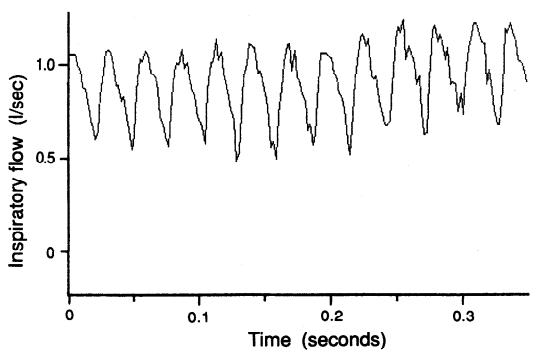

FIG. 8. Mouth $\dot{V}$ during simulated snore. Note asymmetry of $\dot{V}$ oscillations and faster reopening than closure in many waveforms. Oscillation rate was 39 Hz.

Liistro et al. (12), Rauscher et al. (16), Katz et al. (10), and others noted $\dot{V}$ oscillations in the $\dot{V}$ curves of snorers and OSA patients. A review of published tracings, as well as our own data, shows that these $\dot{V}$ oscillations are asymmetric and often reach zero $\dot{V}$ on the downstroke phase of the curve. Note that the measurements of $\dot{V}$ at the airway opening may not adequately represent the $\dot{V}$ value at the oscillating site because of distortion imposed by Rua and the compliance and inertia of the upper airway walls. The phenomenon of $\dot{V}$ oscillation as described and its association to the mechanics of snores needs to be explained. The present model predicts that complete airway collapse and $\dot{V}$ interruption will occur once critical conditions are reached (although it must be pointed out that because $\dot{V}$ is assumed to remain constant, the model may lose validity as wall motion becomes very rapid). This is different from flutter oscillations (5), where the airway walls oscillate around a mean narrowed, yet open, position. The model also enables calculation of the time course for airway closure. For the parameter values of interest, a range of closure times of 0.01–0.1 s was found. We conducted simple qualitative experiments to evaluate these predictions. The high-frequency response $\dot{V}$ measurement helped reveal the true nature of $\dot{V}$ oscillations during snores. The asymmetric pattern with $\dot{V}$ reduction to almost zero is compatible with the model's prediction of complete airway closure in each cycle. It should be noted that although the frequency response of the measuring system was high, the compliance of the soft walls of the mouth limits the total frequency response of the system.

Analyses of snoring sounds from men and from a dog preparation of upper airway obstruction show repetition of sound structures at a rate of 30–100/s (1). These structures correspond to the $\dot{V}$ oscillations measured at the mouth. Thus each sound structure may correspond to a flapping closure and reopening of the upper airways. The rate of appearance of these sound structures, as well as the frequency of the oscillations, is well within the range predicted by the model.

Critical evaluation of model. We were unable to find other models of snoring in the life sciences literature for comparison, although this model contains some features shared by other models describing unsteady $\dot{V}$'s within elastic-walled structures, in particular "lumped-parameter" models describing self-excited oscillations in collapsible tubes (e.g., see Ref. 2). The oscillations predicted by lumped-parameter models are characterized by the fact that the cross-sectional area of the conduit remains nonzero throughout an oscillation, and fundamental to these oscillations is the presence of dissipation in $\dot{V}$ (and possi-

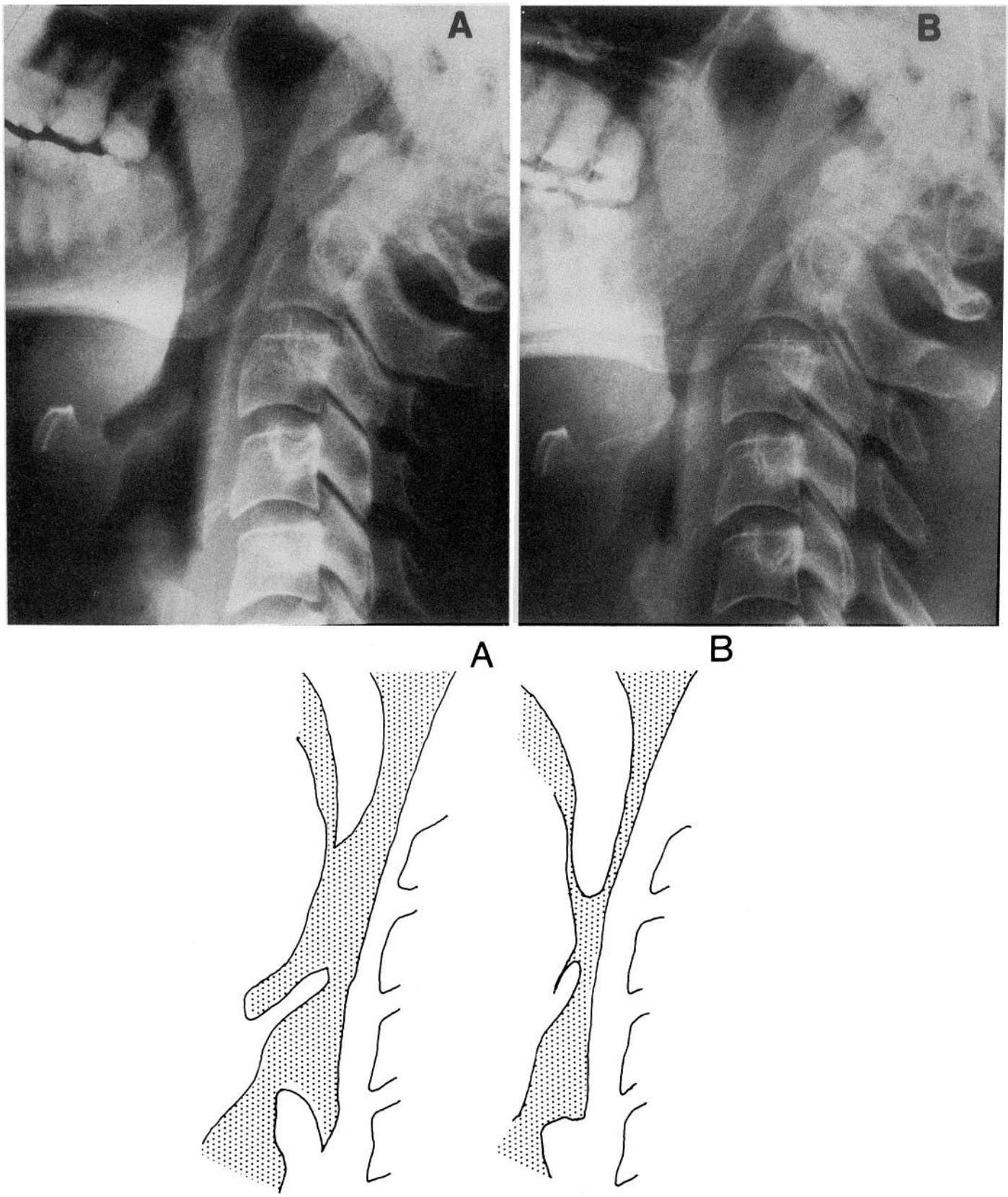

FIG. 9. *Top*: radiographic lateral view of neck during relaxation (*A*) and during −24 cmH_2O static inspiratory effort against closed mouth and nose (*B*). Line tracings of upper airways (*bottom*) demonstrate extent of motion of soft tissues.

bly in the wall), ensuring that unsteady pressure fluctuations and wall displacements are out of phase with one another (5). In the present model we neglect dissipation (except for a rough estimation of the upper airway viscous head loss) so that pressure and displacement remain in phase and the channel is then subject to a nonoscillatory instability leading to complete closure of the channel. Because we assume that $\dot{V}$ through the collapsing segment is independent of time and space, ours is essentially a quasi-steady model, and the neglect of potentially important unsteady terms in the mass and momentum conservation equations will affect the predicted time course of closure. This is not expected to influence the critical conditions that lead to either closure or stability, however.

Choosing W, L, m, and K as free standing independent parameters is clearly unrealistic. In reality, increasing W or L is expected to modify m and possibly K as well. Because m does not play a role in the determination of the critical conditions for closure, it seems reasonable not to include second-order effects in the present form of the model. To the best of our knowledge, the relationships between W, L, and K have not been measured experimentally. Nevertheless, with the use of Fig. 6, C and D, it is possible to evaluate the effect of each of the parameters alone or in combination.

The model assumes uniform b_0 throughout the rectangular collapsible segment. Clearly, this is an oversimplification of the problem, since the upper airway walls do not remain parallel at all times. Had we taken K to be a distributed, rather than a lumped, parameter, the pressure drop due to viscous resistance across the collapsible segment would have caused a tilt and a nonuniform closure. In addition, treatment of the potential effects of nonparallel airway wall on convective acceleration forces and of the changing values of b on the flow regime would have made the model more realistic but was avoided in the simple model presented here.

The predictions of the model are based on the assumption of linear elasticity. Nonlinear elastic effects, represented, for example, by an airway "tube law" that is similar to that described for the bronchial airways, may be handled in the model by replacing $1 - b$ with $1 - b + \epsilon b^{-3}$ in *Eq. 4*. If ϵ is small, then as q increases through q_c, the solution jumps from b_2 to a solution with smaller b. With ϵ larger, there is a smooth transition to this small b solution. That is to say, it is possible to have an incomplete collapse of the airways without closure.

Conclusions. On the basis of the predictions of this simple model, we conclude that instability leading to airway closure is likely to occur once a boundary, determined by the parameters of the system, is passed. Increasing the inspiratory $\dot{V}$ sufficiently is predicted to always cause crossing of the boundary and instability. Narrowing of the collapsible region of the upper airway, increasing its compliance or length, increasing the upper airway viscous resistance, and increasing the density of the breathed gas are all expected to lower the critical threshold and promote instability. According to the model, there exists an optimal airway width such that extensive narrowing or widening of the lateral dimension of the segment is expected to lower the boundary for instability. Using baseline parameter values taken from the literature and from simple experiments reported here, we showed that transition from stable to unstable conditions is possible for relatively small (i.e., 2-fold) changes in the parameters, well within the range of clinically encountered values. The power relationships between the parameters show that the effect of $\dot{V}$ is dominant (i.e., power = 3). The length, diameter, and elastance of the collapsible segment are second in importance (i.e., power = 2), whereas the effects of Rua and ρ are the least significant (i.e., power = 1).

We thank Hope Bailot for assistance with the radiographic study. Drs. A. Oliven, M. Odeh, and R. Beck participated in the measurements of the snoring sounds.

This study was supported by the United States-Israel Binational Science Foundation; National Heart, Lung, and Blood Institute Grants K04-HL-01818 and R01-HL-41126; and National Science Foundation Grant CTS-9013083 (to J. B. Grotberg).

Address for reprint requests: N. Gavriely, Pulmonary Physiology Unit, Faculty of Medicine, Technion-IIT, PO Box 9697, Haifa, Israel.

Received 21 November 1991; accepted in final form 14 January 1993.

REFERENCES

1. BECK, R., N. GAVRIELY, M. ODEH, AND A. OLIVEN. Time expanded waveform and spectral characteristics of snores in a dog model of upper airway obstruction (Abstract). *Am. Rev. Respir. Dis.* 139: A181, 1989.
2. BERTRAM, C. D., AND T. J. PEDLEY. A mathematical model of unsteady collapsible tube behavior. *J. Biomech.* 15: 39–50, 1982.
3. CHADWICK, G. A., P. CROWLEY, M. X. FITZGERALD, R. G. O'REGAN, AND W. T. MCNICHOLAS. Obstructive sleep apnea following topical oropharyngeal anesthesia in loud snorers. *Am. Rev. Respir. Dis.* 143: 810–813, 1991.
4. GLEADHILL, I. C., A. R. SCHWARTZ, N. SCHUBERT, R. A. WISE, S. PERMUTT, AND P. L. SMITH. Upper airway collapsibility in snorers and in patients with obstructive hypopnea and apnea. *Am. Rev. Respir. Dis.* 143: 1300–1303, 1991.
5. GROTBERG, J. B., AND N. GAVRIELY. Flutter in collapsible tubes: a theoretical model of wheezes. *J. Appl. Physiol.* 66: 2261–2272, 1989.
6. HOFFSTEIN, V., W. WEISER, AND R. HANEY. Roentgenographic dimensions of the upper airway in snoring patients with and without obstructive sleep apnea. *Chest* 100: 81–85, 1991.
7. HOFFSTEIN, V., S. WRIGHT, N. ZAMEL, AND T. D. BRADLEY. Pharyngeal function and snoring characteristics in apneic and nonapneic snorers. *Am. Rev. Respir. Dis.* 143: 1294–1299, 1991.
8. HUDGEL, D. W., C. HENDRICKS, AND H. B. HAMILTON. Characteristics of the upper airway pressure-flow relationship during sleep. *J. Appl. Physiol.* 64: 1930–1935, 1988.
9. JORDAN, D. W., AND P. SMITH. *Nonlinear Ordinary Differential Equations.* New York: Clarendon, 1977.
10. KATZ, I., N. ZAMEL, A. S. SLUTSKY, A. S. REBUCK, AND V. HOFFSTEIN. An evaluation of flow-volume curves as a screening test for obstructive sleep apnea. *Chest* 98: 337–340, 1990.
11. LIISTRO, G., D. STANESCU, G. DOOMS, D. RODENSTEIN, AND C. VERITER. Head position modifies upper airway resistance in men. *J. Appl. Physiol.* 64: 1285–1288, 1988.
12. LIISTRO, G., D. STANESCU, AND C. VERITER. Pattern of simulated snoring is different through mouth and nose. *J. Appl. Physiol.* 70: 2736–2741, 1991.
13. LUGARESI, E., F. CIRIGNOTTA, G. COCCAGNA, AND P. MONTAGNA. Clinical significance of snoring. In: *Sleep and Breathing,* edited by N. Saunders and C. Sullivan. New York: Dekker, 1984, vol. 21, p. 283–298. (Lung Biol. Health Dis. Ser.)

14. PEREZ-PADILLA, R., AND J. E. REMMERS. Dynamics of pressure, airflow and noise production during simulated snoring (Abstract). *Am. Rev. Respir. Dis.* 131: 106, 1985.
15. POLO, O. J., M. TAFTI, J. FRAGA, K. V. PORKKA, Y. DEJEAN, AND M. BILLIARD. Why don't all heavy snorers have obstructive sleep apnea? *Am. Rev. Respir. Dis.* 143: 1288–1293, 1991.
16. RAUSCHER, H., W. POPP, AND H. ZWICK. Flow-volume curves in obstructive sleep apnea and snoring. *Lung* 168: 209–214, 1990.
17. REMMERS, J. E., T. FEROAH, R. PEREZ-PADILLA, AND W. A. WHITELAW. Correlation of structure and mechanics in pharyngeal obstruction during sleep. In: *Chronic Rhonchopathy,* edited by C. H. Chouard. Paris: Libbey, 1987, p. 30–35.
18. RODENSTEIN, D. O., G. DOOMS, Y. THOMAS, G. LIISTRO, D. C. STANESCU, C. CULEE, AND G. AUBERT-TULKENS. Pharyngeal shape and dimensions in healthy subjects, snorers and patients with obstructive sleep apnea. *Thorax* 45: 722–727, 1990.
19. SCHAFER, J., AND W. PIRSIG. Digital analysis of snoring sounds in children. *Int. J. Pediatr. Otorhinol.* 20: 193–202, 1990.
20. SULLIVAN, C. E., F. G. ISSA, M. BERHON-JONES, AND L. EVES. Reversal of obstructive sleep apnea by continuous positive airway pressure applied through the nares. *Lancet* 1: 862–865, 1981.
21. SURATT, P. M., S. C. WILHOIT, AND K. COOPER. Induction of airway collapse with subatmospheric pressure in awake patients with sleep apnea. *J. Appl. Physiol.* 57: 140–146, 1984.
22. WHITE, D. P. Occlusion pressure and ventilation during sleep in normal humans. *J. Appl. Physiol.* 61: 1279–1287, 1986.